Entropy-driven transition in a one-dimensional system

Thierry Dauxois and Michel Peyrard
Laboratoire de Physique, Ecole Normale Supérieure de Lyon, CNRS URA 1325, 46 allée d'Italie, 69007 Lyon, France
(Received 21 December 1994)

We investigate the statistical mechanics of a one-dimensional model with nearest-neighbor interactions and a substrate potential that exhibits an entropy-driven transition. Approximate analytical results obtained with the second-order self-consistent phonons method are presented. Two different numerical methods are used to derive exact numerical results for the thermodynamical functions. Finally, we discuss the important features of the Hamiltonian, which are responsible for this phase transition.

PACS number(s): 05.20.−y, 63.70.+h, 64.70.−p, 05.90.+m

I. INTRODUCTION

Although the theory of phase transitions has been at the heart of statistical physics studies for several decades, there are still many unsolved questions, particularly for first-order phase transitions. Recently there has been a renewal of interest in such transitions that has been initiated by new models of structural phase transitions, especially martensitic transitions in metallurgy [1–5]. These transitions do not show a soft-mode behavior and their physics is characterized by intrinsic nonlinear features and *quasiharmonic concepts are not applicable.*

First-order temperature-driven transitions can be found in systems where the bulk entropy changes at the transition. They have been called *entropy-driven phase transitions* [2,6] and they have been studied in two-dimensional models by numerical simulations [7], by mean-field theory [6], or through the exact results that can be obtained from transfer-matrix calculations in lattices that have a finite breadth in one direction [4,8].

In order to understand the mechanism of entropy-driven transitions and the conditions that a system must fulfill to exhibit such a transition, it would be very interesting to have a simple model, such as a *one-dimensional model.* The absence of phase transitions in one-dimensional systems with finite-range interactions is so often quoted that it may seem impossible to develop such a model. However, there are counterexamples to this statement. Temperature-driven phase transitions in one-dimensional systems are known in chains made of elements having a finite number of states and for which the partition function has a simple expression as a function of the internal states of the elements [9,10]. For systems of interacting particles in one dimension, Van Hove gave a proof that there is no transition [11], but his calculation uses the fact that the partition function can be written in terms of difference of atomic coordinates. This is the case when the potential energy is due only to interatomic interactions, but it is no longer true in the presence of a field or with an external potential applied to each particle. Moreover there are real quasi-one-dimensional systems that exhibit a phase transition. This is the case of the "melting" transition of DNA, i.e., the thermal denaturation during which the two strands of the double helix separate from each other [12] when the molecule is heated above about 340 K. In fact, this problem motivated one of the work on quasi-one-dimensional systems having a transition cited above [10]. In DNA models an "on-site" potential occurs naturally due to the interaction between the two strands [13] and the Van Hove calculation does not apply.

Recently, we proposed [14] a model in which the cooperative effects, which had been introduced phenomenologically in the Ising models of DNA denaturation, are introduced at the microscopic level by an appropriate anharmonic stacking interaction potential that reflects the change in the electronic distribution on the bases when hydrogen bonds are broken. With this interaction the system shows a very sharp melting transition. Besides its interest for DNA, this model provides an *interesting example of entropy-driven transition in a one-dimensional system.* This paper is devoted to the study of this transition. Although we cannot claim that it is a true first-order transition, it exhibits close similarities with such a transition. Our aim here is to discuss the origin of this particular behavior.

Our model can be considered as a simple extension of the Ising models for DNA denaturation. Instead of a two-state variable, the status of each base pair n is described by a scalar variable y_n representing the transverse stretching of the hydrogen bonds connecting the two bases. The Hamiltonian is

$$H = \sum_n \left[\frac{1}{2} m \dot{y}_n^2 + D(e^{-a y_n} - 1)^2 + W(y_n, y_{n-1}) \right]. \quad (1)$$

The first term is the kinetic energy term for bases of mass m. The on-site Morse potential represents not only the H bonds connecting two bases belonging to opposite strands, but also the repulsive interactions of the phosphates and the surrounding solvent effects. This potential is due to the presence of two chains in DNA [13] and has the same effects as an external field. The stacking energy between two neighboring base pairs is described by the anharmonic potential

$$W(y_n, y_{n-1}) = \frac{K}{2}\left(1 + \rho e^{-\alpha(y_n + y_{n-1})}\right)(y_n - y_{n-1})^2. \quad (2)$$

This intersite coupling, replacing the simple harmonic coupling of our first approaches [15,13], is the essential feature of the model and it is responsible for its interesting properties. The choice of this potential has been motivated by the observation that the stacking energy is not a property of *individual* bases, but a character of the base *pairs* themselves [16]. With the W coupling term, the effective coupling constant decreases from $K(1+\rho)$ to K, when either one of the two interacting base pairs is stretched, in qualitative agreement with the experimental motivation of this work. The anharmonic coupling term does not correspond to a renormalization of the Hamiltonian and, in the model, the parameter ρ and the coupling constant K are not temperature dependent. We showed in previously published work [17] how the mechanism of discreteness-induced energy localization could appear in a large variety of systems involving lattices. Numerical simulations of the model at constrained temperature show [13] that, in the steady state, thermal energy tends to localize itself around some sites. This process initiates the formation of small amplitude breathing modes, which grow by an energy exchange mechanism between the nonlinear excitations and create the precursor events of the transition.

The paper is organized as follows. Section II introduces the statistical mechanics of the model. In Sec. III a self-consistent phonon theory is used to derive analytical expressions of thermodynamical functions in the low and high temperature range. We devote Sec. IV to a detailed study of the phase transition and show first how we can obtain the exact thermodynamical functions with two differents methods; then we discuss the possible reasons that give this phase transition in Sec. V.

II. STATISTICAL MECHANICS

Since the model is one dimensional and because the interactions are restricted to nearest-neighbor interactions, its statistical mechanics can be treated exactly, including fully the nonlinearities, with the transfer operator method [15]. This is one major interest of this system as a model to study entropy-driven phase transitions.

For a chain containing N units, the classical partition function, given in terms of the Hamiltonian (1), may be factored as

$$\mathcal{Z} = \int \prod_{n=1}^{N} dy_n dp_n e^{-\beta H_y} = \mathcal{Z}_p \, \mathcal{Z}_y. \tag{3}$$

The integral over the momenta $p_n = m y_n$ is a Gaussian integral and gives the familiar kinetic factor for N particles $\mathcal{Z}_p = (2\pi m k_B T)^{N/2}$. With a coupling limited to nearest-neighbor interactions, $\mathcal{Z}_y$ can be expressed in the form

$$\mathcal{Z}_y = \int_{-\infty}^{+\infty} \prod_{n=1}^{N} dy_n e^{-\beta f(y_n, y_{n-1})}, \tag{4}$$

where f denotes the potential energy of the Hamiltonian (1) relative to the nth site.

Since it has been introduced to describe DNA thermal denaturation, the model has been the subject of some debate in the literature [18,19]. The problem is the definiteness of the partition function because the on-site potential $V(y_n) = D(e^{-ay_n} - 1)^2$ is bounded for $y_n \to \infty$. The integrand of Z_y decays exponentially to zero for large y_n almost everywhere because the coupling term diverges as y^2. However, there is *one* trajectory in the phase space for which this is not true. If all the y_n tend to infinity while staying always equal to each other, the coupling term is identical to zero and the integrand of Z_y does not vanish. This is a familiar situation in physics because the requirement that all y_n stay equal simply corresponds to the translational mode of the system, which is known to cause a divergence in the partition function of a translationally invariant system. Usually this mode is simply excluded by removing the center of mass degree of freedom in the definition of the partition function [20]. In our case, however, the situation is not exactly the same because, due to the on-site Morse potential, the system is not invariant with respect to a global translation along y. The stability of the model is only obtained in the thermodynamic limit because the weight in the phase space of the particular trajectory where all y are equal becomes negligible. This can be understood by looking at small systems. Consider first a *single* Morse oscillator in equilibrium with a thermal bath. It escapes to infinity at any temperature because the thermal fluctuations have a nonvanishing probability to bring the oscillator on the flat part of the potential. Then there is almost no restoring force and the amplitude of the motion can diverge, although the divergence is very slow for $kT \ll D$. This phenomenon can easily be tested by numerical simulations. If we consider now a small number N_0 of such oscillators that are harmonically coupled, the time required for the divergence increases very fast with N_0 because if the fluctuations bring one oscillator on the flat part of the Morse potential, the coupling with its neighbors tend to bring it back, unless the neighbors are simultaneously on the plateau of the potential. Therefore the probability to actually follow the diverging trajectory decays very fast with N_0 and, in the thermodynamic limit, the system is stable for an infinite time.

In order to avoid a possible technical problem with the global translational mode and to make sure that we work with a problem that is mathematically well posed, we shall bound the variation of y by a constant A, i.e., we restrict the phase space to $-\infty < y_n < A$. The introduction of such a cutoff is also required in the numerical calculation of the partition function, which is discussed in Sec. IV. Then we shall study the properties of the system as a function of A and show that the limit $A \to \infty$ is well defined. In addition, the analytical and the numerical calculations will be done with periodic boundary conditions.

III. SELF-CONSISTENT PHONONS METHOD

As the analytical calculations of the partition functions are not tractable, before using numerical methods to cal-

culate the partition function, let us use the self-consistent phonons (SCP) method to obtain approximate analytical results in the low and high temperature regimes in order to understand the denaturation mechanism better. First, in the high temperature regime the whole system is on the plateau of the Morse potential, with an effective harmonic coupling constant K. Therefore, since the system is equivalent to a harmonic chain, without substrate potential we expect its free energy to be simply

$$\mathcal{F}_y = -\frac{k_B T}{2} \sum_{p=1}^{N-1} \ln \frac{\pi k_B T}{2K \sin^2(\frac{\pi p}{N})} \tag{5}$$

and the specific heat per particle in units of k_B will be equal to 1. Figures 1 and 6(b) show that, above the transition, this picture is correct.

In the low temperature regime, introducing $u_n = y_n - \langle y \rangle = y_n - \eta$ and two variational parameters Ω^2 and ϕ, we apply the SCP method [5,13] by considering the trial harmonic Hamiltonian

$$H_0 = \sum_n \left[\frac{1}{2} m \dot{u}_n^2 + \frac{\phi}{2}(u_n - u_{n+1})^2 + \frac{\Omega^2}{2} u_n^2 \right]. \tag{6}$$

At first order, the free energy of the system is bounded from above by [21]

$$\mathcal{F} \leq -k_B T \ln \mathcal{Z}_0 + \langle H - H_0 \rangle$$

$$= -\frac{k_B T}{2} \sum_{p=0}^{N-1} \ln \frac{2\pi k_B T}{\Omega^2 + 4\phi \sin^2(\frac{\pi p}{N})} + \mathcal{F}_1, \tag{7}$$

where $\mathcal{Z}_0$ is the partition function for the trial Hamiltonian and the mean value is calculated with this approximate Hamiltonian. Minimizing expression (7) with respect to η, $\langle u^2 \rangle = \langle u_n^2 \rangle$, and $\langle v^2 \rangle = \langle u_n u_{n-1} \rangle$, we obtain five equations, which have to be solved self-consistently:

$$\langle u^2 \rangle = \frac{k_B T}{N} \sum_q \frac{1}{\Omega^2 + 4\phi \sin^2(\frac{q}{2})}, \tag{8}$$

$$\langle v^2 \rangle = \frac{k_B T}{N} \sum_q \frac{\cos(q)}{\Omega^2 + 4\phi \sin^2(\frac{q}{2})}, \tag{9}$$

$$\phi = K\{1 + \rho e^{-2a\eta + \alpha^2(\langle u^2 \rangle + \langle v^2 \rangle)}[1 - \alpha^2(\langle u^2 \rangle - \langle v^2 \rangle)]\}, \tag{10}$$

$$\Omega^2 = 2aD\Big[2(a-\alpha)e^{-2a\eta + 2a^2\langle u^2 \rangle} + (2\alpha - a)e^{-a\eta + \frac{a^2}{2}\langle u^2 \rangle}\Big], \tag{11}$$

$$0 = \alpha K \rho(\langle u^2 \rangle - \langle v^2 \rangle) e^{-2a\eta + \alpha^2(\langle u^2 \rangle + \langle v^2 \rangle)} - aD\Big[-e^{-2a\eta + 2a^2\langle u^2 \rangle} + e^{-a\eta + \frac{a^2}{2}\langle u^2 \rangle}\Big]. \tag{12}$$

This system has a solution only for $T \leq T_0$, where T_0 is a characteristic temperature that appears as the transition temperature for the SCP calculation. The resulting first-order expression for the free energy is

$$\mathcal{F}_1 = \langle H - H_0 \rangle = D + De^{-a\eta + \frac{a^2}{2}\langle u^2 \rangle}\Big[(a^2 + a\alpha)\langle u^2 \rangle - a\alpha\langle v^2 \rangle - 2\Big] + De^{-2a\eta + 2a^2\langle u^2 \rangle}\Big[-(a\alpha + 2a^2)\langle u^2 \rangle + a\alpha\langle v^2 \rangle + 1\Big]. \tag{13}$$

As shown in Fig. 1, the agreement with the exact transfer-integral (TI) result is poor except at very low temperature because, given the even parity of H_0, the first-order expression of $\mathcal{F}$ averages out all the odd terms of the Morse potential. Although the calculation is tedious, the second-order correction to the free energy [21,5]

$$\mathcal{F}_2 = -\frac{\langle (H - H_0)^2 \rangle - \langle H - H_0 \rangle^2}{2k_B T} \tag{14}$$

can be calculated analytically exactly for our model (see the Appendix). Then, we have an explicit analytical approximate expression of the second-order correction to the free energy. Figure 1 shows that it significantly improves the agreement with the exact results. However, the SCP calculations still fails in the vicinity of the melting transition, emphasizing the fundamental role of the nonlinear effects in the denaturation: they cannot be described, even approximately, by a harmonic trial Hamiltonian with temperature dependent coefficients.

We have also developed a mean field theory for this model [22]. We used the modificated and extended theory

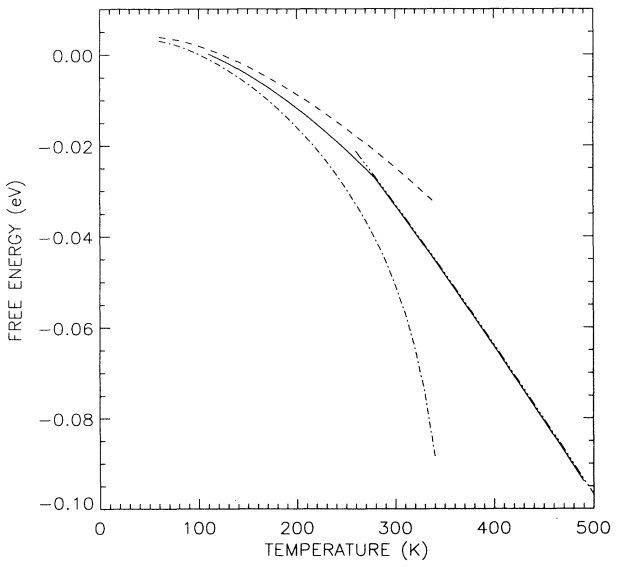

FIG. 1. Variation of the free energy vs temperature. The solid line corresponds to the exact free energy calculated with the transfer integral operator, the dashed line corresponds to first-order SCP result $\mathcal{F}_0 + \mathcal{F}_1$, the dash-dotted line corresponds to the second-order SCP result $\mathcal{F}_0 + \mathcal{F}_1 + \mathcal{F}_2$, and the dash–triple-dotted line corresponds to the high-temperature harmonic approximation. The parameters are $\alpha = 0.35$, $D = 0.03$ eV, $a = 4.5$ Å^{-1}, $K = 0.06$ eV/Å, $\rho = 1$, and $m = 300$ amu.

introduced by Kerr and Rave [6], which assumes that the particles move independently and that the single-particle probability distribution for the displacements is a Gaussian function. We can then obtain two parameters, the average displacement and its mean square fluctuation. Then we can compute the averaged free energy per particle and finally, minimizing the free energy versus the two parameters, we derive the solution of the mean field theory. It qualitatively agrees with the exact numerical technique, presented in the next section, but provides neither an exact result nor an additional qualitative understanding of the transition.

IV. PHASE TRANSITION

A. Transfer integral operator

1. Standard technique

As the approximate analytical calculations using the SCP method and the mean field theory are not sufficient to describe the transition, we will exactly evaluate the integral (4) in the thermodynamic limit of a large system ($N \to \infty$) using the eigenfunctions and eigenvalues of the transfer integral operator [23–25,4]

$$\int dy_{n-1} \exp\Big[-\beta\Big(W(y_n, y_{n-1}) + \frac{1}{2}\big[V(y_{n-1}) + V(y_n)\big]\Big)\Big]\phi_i(y_{n-1}) = e^{-\beta\varepsilon_i}\phi_i(y_n), \tag{15}$$

where, as discussed in Sec. II, all integrations are performed in the domain $-\infty < y_n < A$. The calculation is similar to the one performed by Krumhansl and Schrieffer [24] for the statistical mechanics of the ϕ^4 field. It yields $\mathcal{Z}_y = \exp(-N\beta\varepsilon_0)$, where ε_0 is the lowest eigenvalue of the operator. The lattice effects in this case go certainly beyond perturbation corrections [26] and standard analytical methods cannot be used. Therefore we have solved numerically without approximations the eigenvalue equation of the transfer operator [27]. We used two different and independent methods to reach this goal.

First, we can symmetrize the transfer integral operator and replace the integral by sums of discrete increments, using summation formulas at different orders. The problem is then equivalent to finding the eigenvalues and the eigenvectors of a symmetric matrix.

Using Eq. (15) and the orthonormalization property

$$\int \phi_n^*(y)\phi_m(y)\, dy = \delta_{nm} \tag{16}$$

we obtain an expression with a structure similar to that of the eigenvalue problem

$$\sum_i \sum_j M_{i,j} b_i b_j = \lambda, \tag{17}$$

if we replace the integrals by sums of discrete increments. For practical purposes, the summation is restricted to a finite number of points, chosen so that the eigenvalue is sufficiently accurate. We used the following different methods to discretize the integral: the trapezoidal rule, the Simpson rule, and Bode's integration rules of order 6 and 10. The last one gives the best accuracy. We are using 1441× 1441 matrices.

2. Kellog's method

However, since we are interested in just the three first eigenvalues, faster algorithms are more appropriate in our case. The simplest one is the Kellog's method for solving symmetric integral equations [28]. Starting with an arbitrary normalized function $\varphi_0(s)$ we determine the normalized functions $\varphi_\nu(s)$ and the numbers λ_ν from the relation

$$\varphi_{\nu+1}(s) = \lambda_{\nu+1} \int K(s,t)\, \varphi_\nu(t)\, dt. \tag{18}$$

The passage to the limit can be carried out and leads to an eigenvalue $\lambda_\infty = e^{\beta\varepsilon_0}$ and associated normalized eigenfunction $\varphi_\infty = \phi_0$ of the kernel. Practically, we define a convergence criterion to test the accuracy of the eigenvalue. Once the lowest eigenvalue ε_0 has been obtained, it is possible to construct a new kernel K_1, orthogonal to K and still symmetric:

$$K_1(s,t) = K(s,t) - e^{\beta\varepsilon_0}\, \phi_0(s)\phi_0(t). \tag{19}$$

Then, we derive the lowest eigenvalue of this kernel, which corresponds to the first excited eigenvalue of the original kernel K. Of course, we can apply this technique several times to obtain successively the eigenvalues in increasing order.

Practically, we have to choose trial eigenfunctions, in order to initiate the iterative process. As we expect one localized eigenfunction for the fundamental eigenstate and delocalized functions for the two first excited states, we have chosen a Gaussian around $y = 0$ for the first one and cosine functions for the two others. With this choice, we check that the system converges quite rapidly toward the exact eigenfunctions. We checked that the results do not depend upon this choice as predicted by the convergence of the process. For instance, the localized solution is also found if we start from a nonlocalized sinusoidal trial function, at the expense of a larger number of convergence steps. The eigenfunctions obtained are then used as initial conditions for the iterative process corresponding to the next temperature step.

B. Results

With these methods, we were able to compute the three lowest eigenvalues of the transfer integral operator and therefore all the consequent thermodynamical functions. The two methods are numerical, but completely indepen-

dent, and gave the same results. The parameters of the model are a dissociation energy $D = 0.03$ eV, a spatial scale factor of the Morse potential $a = 4.5$ Å^{-1}, a coupling constant $K = 0.06$ eV/Å^2, and a mass $m = 300$ amu. We used an accuracy criterion fixed to 10^{-8}.

In this section we will first show the fundamental difference of behavior in the harmonic case ($\alpha = 0$) and in the anharmonic case ($\alpha = 0.35$). Indeed, as pointed out in a previous paper [13], although it goes far beyond the Ising model in its ability to describe the dynamics of the DNA denaturation, the harmonic model is still not sufficient because it predicts a denaturation that occurs at a too high temperature and in addition extends over a too large temperature region. This remark motivated the modification of the model to introduce cooperativity effects in terms of a nonlinear contribution to the base-pair stacking interaction; this results in a dramatic change of the mean value $\langle y \rangle$ versus temperature. Figures 2(a) and 2(b) show the evolution of $\langle y \rangle$ in both cases. We note that, if $\langle y \rangle$ goes slowly toward infinity in the harmonic case, the anharmonic case gives rise to an extremely sharp transition [29], reminiscent of a first-order phase transition.

One major point is to check that the results are independent of the limits of the integral. The exponential increase of the Morse potential for negative value of y allows us to take a rather small value for the lower limit of the interval because the function that we integrate decays

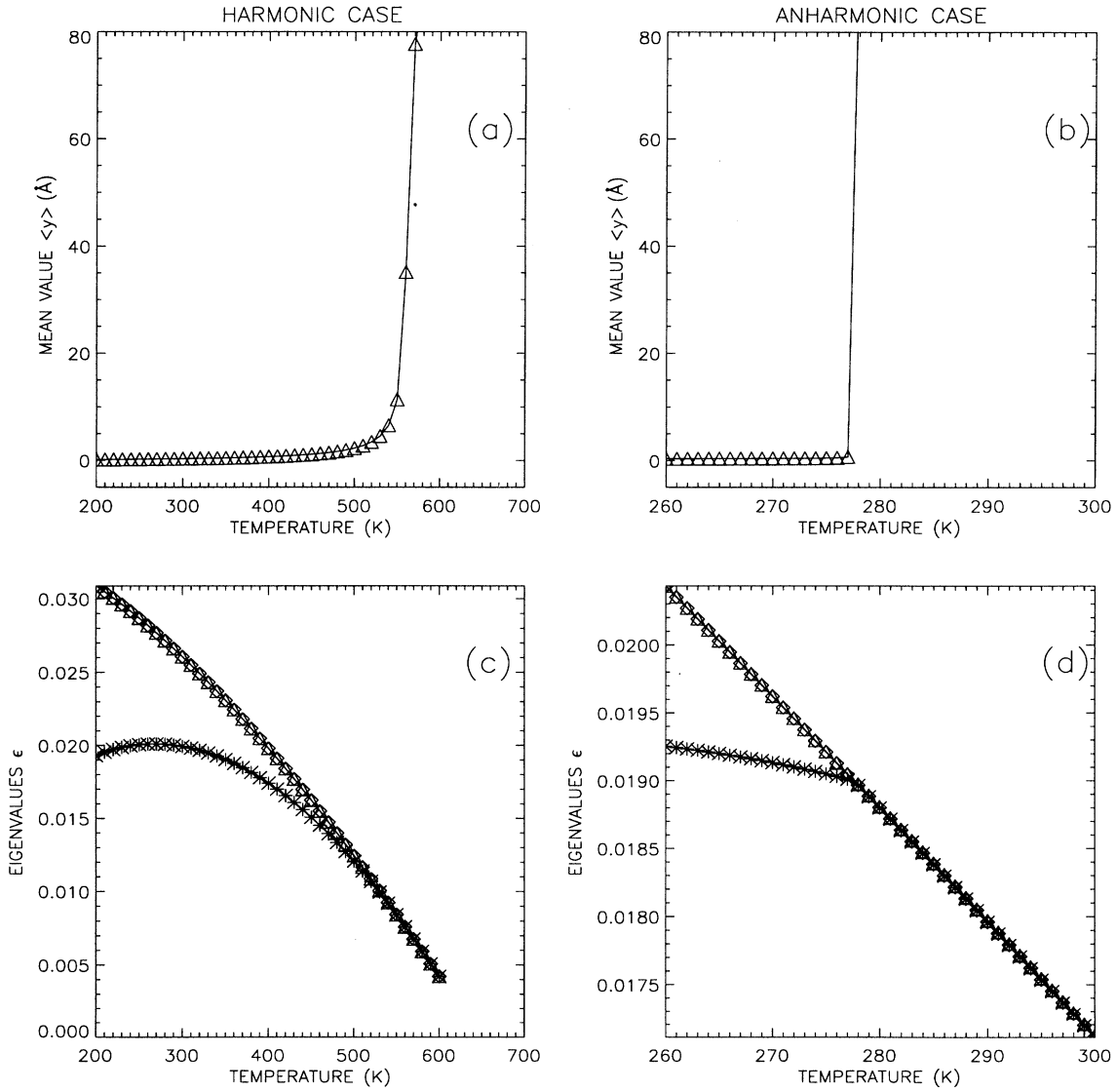

FIG. 2. Comparison of the harmonic case and the anharmonic case. (a) and (c) correspond to the harmonic case ($\alpha = 0$), whereas (b) and (d) correspond to the anharmonic case ($\alpha = 0.35$). (a) and (b) present the evolution of the mean value $\langle y \rangle$ vs temperature. (c) and (d) present the evolution of the three lowest eigenvalues of the transfer integral operator vs temperature. The asterisk corresponds to ε_0, the diamond to ε_1, and the triangle to ε_2. The parameters are $D = 0.03$ eV, $a = 4.5$ Å^{-1}, $K = 0.06$ eV/Å, $\rho = 1$, and $m = 300$ amu.

extremely fast for $y < 0$. To determine the upper limit, we study the value of the critical temperature versus the upper limit of integration A. When A is small (for instance, $A = 20$ Å), the transition is not as sharp as it is for the cases shown in Fig. 2(b), but it generates a peak in the specific heat. The temperature corresponding to this peak is taken as the critical temperature. The calculations are made in the anharmonic case, where the peak is well defined and not broad as it is in the harmonic case. Given the domain of integration, we chose the number of increments to work with a constant numerical resolution. In order to have a better extrapolation for an infinite value of A, it is convenient to introduce a fitting parameter δ in order to obtain a straight line: therefore we plot T_c versus A^δ on Fig. 3. The value 2.2 for δ is appropriate. We note that the value of the critical temperature converges, rather rapidly, toward a finite value (here $T_c = 277.5$) when the upper limit of integration is $A \simeq 100$. The spatial domain of resolution that we chose for all the calculations presented below is [−5 Å,+195 Å] divided into 1440 steps.

The transition appears also in the spectrum of the transfer integral operator (see Fig. 4). Below T_c, the operator has a discrete eigenvalue $\varepsilon_0(T)$ separated from a continuum, while above T_c the discrete eigenvalue has disappeared. On the figure the continuum appears as a set of discrete values that extends above a lower limit $\varepsilon_c(T)$ because of the limited resolution of the numerical integration (in our calculation the "continuum" contains 1440 values ranging from ε_c to $+\infty$).

What is important in our model is the way the discrete eigenvalue disappears. As shown on Fig. 4, the curve $\varepsilon_0(T)$ penetrates abruptly in the continuum, which means that, at $T = T_c$, the transfer integral operator has

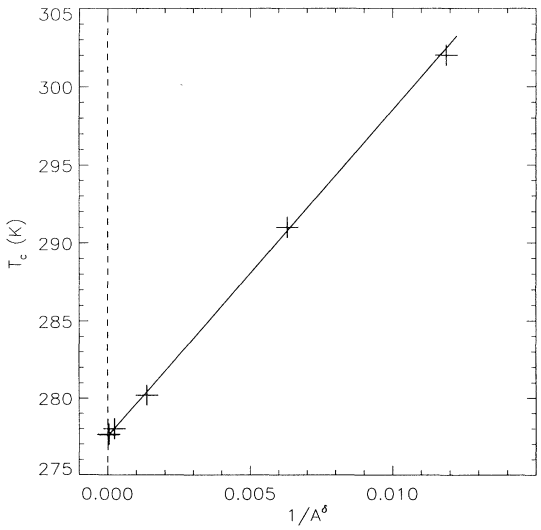

FIG. 3. Value of the critical temperature (defined by the peak of the specific heat) versus $1/A^\delta$, where A is the upper bound of the integral. The five different points correspond to $A = 195, 95, 45, 20, 10$, and 7.5. The fitting parameter δ is 2. The parameters are $\alpha = 0.35$, $D = 0.03$ eV, $a = 4.5$ Å^{-1}, $K = 0.06$ eV/Å, $\rho = 1.0$, and $m = 300$ amu.

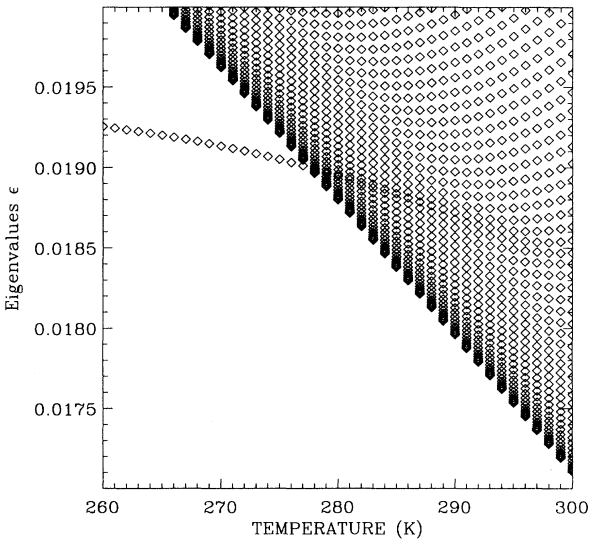

FIG. 4. Spectrum of the transfer integral operator as a function of temperature. The parameters are $D = 0.03$ eV, $a = 4.5$ Å^{-1}, $K = 0.06$ eV/Å, $\rho = 1$, and $m = 300$ amu.

degenerate eigenvalues. The degeneracy is not only attested by the sharpness of the crossing between the curves $\varepsilon_0(T)$ and $\varepsilon_c(T)$, but also because the penetration of the curves $\varepsilon_0(T)$ inside the continuum leaves in the continuum part of the spectrum a "footprint" that can be observed on Fig. 4 as a local increase in the density of states along the direction that the curve $\varepsilon_0(T)$ was following at $T < T_c$.

The differences between the harmonic and the anharmonic case can be understood more clearly by plotting on Figs. 2(c) and 2(d) the three lowest eigenvalues of the TI operator, computed numerically when $\alpha = 0$ and $\alpha = 0.35$. Contrary to the anharmonic case discussed above where $\varepsilon_0(T)$ has a sharp intersection with the lower limit of the continuum [Fig. 2(d)], in the harmonic case $\varepsilon_0(T)$ tends smoothly to the lower band edge [Fig. 2(c)]. The transition shows up also in the shape of the eigenfunctions of the transfer operator. The functions ϕ_0 corresponding to the lowest eigenvalue is particularly important because $|\phi_0(y)|^2$ gives the probability density for the calculation of $\langle y \rangle$.

Figures 5(a)–5(c) are very helpful to understand the behavior of the system. For $\alpha = 0.35$, they show the three eigenfunctions, corresponding to the three lowest eigenvalues. Because of the finite domain, we note first that the eigenfunctions vanish outside of the interval [−5,195]. But the eigenfunctions are qualitatively different. Below the denaturation temperature T_c, the first eigenfunction ϕ_0 has a sharp peak around $y = 0$; it is a localized function, whereas the two first excited eigenfunctions are delocalized and agree with the standard shape of eigenfunctions in a quantum mechanical problem. The existence of a localized eigenfunction that decays exponentially for large y is important because it confirms the stability of the model in the low temperature range as discussed in Sec. II. As this function is the weighting factor for the

calculation of $\langle y \rangle$, its shape indicates that $\langle y \rangle$ must be finite. Furthermore, because it decays very fast for large y, its determination is not affected by the upper bound of the integral of the transfer operator. This result completes and confirms the results of Fig. 3. Above T_c, the three eigenfunctions associated with the lowest eigenvalue have taken the sinusoidal shape expected for functions belonging to the continuum. They have in addition a small extra peak around $y = 0$, which is a "memory" of the localized state that exists for $T < T_c$.

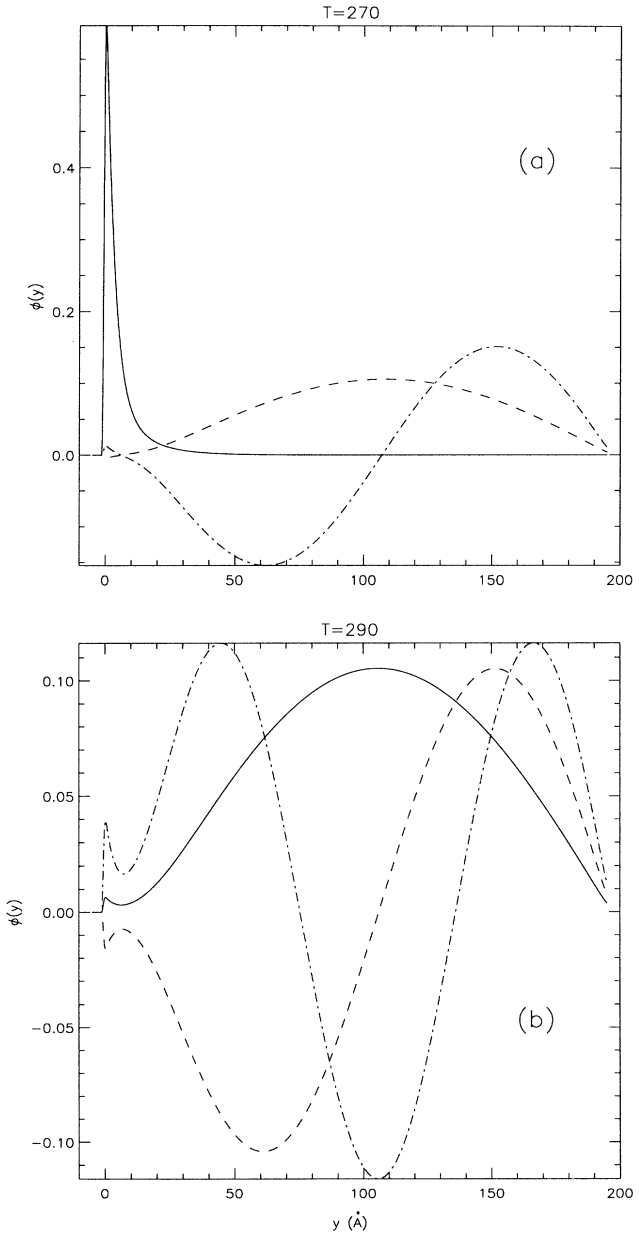

FIG. 5. Eigenfunctions corresponding to the three lowest eigenvalues of the transfer integral operator, before and after the transition. (a) corresponds to $T = 277$ K, (b) to $T = 282$ K, and (c) to $T = 290$ K. The solid line corresponds to ϕ_0, the dashed line to ϕ_1, and the dash-dotted line to ϕ_2. The parameters are $\alpha = 0.35$, $D = 0.03$ eV, $a = 4.5$ Å^{-1}, $K = 0.06$ eV/Å, $\rho = 1$, and $m = 300$ amu.

V. ENTROPY-DRIVEN TRANSITION

In this section we will analyze the process leading to the transition. Our calculations were done in the canonical ensemble, where it is straightforward to derive explicitly the thermodynamical functions, starting from the partition function. For the free energy, it reads

$$\mathcal{F} = -k_B T \ln(\mathcal{Z}_p \mathcal{Z}_y) = -\frac{N k_B T}{2} \ln(2\pi m k_B T) + N\varepsilon_0. \tag{20}$$

We can also derive the energy per site

$$\frac{U}{N k_B} = T\left(\frac{1}{2} - T\frac{\partial \varepsilon_0}{\partial T}\right) \tag{21}$$

and the specific heat

$$\frac{C_V}{N k_B} = \frac{1}{2} - \frac{T}{k_B}\frac{\partial^2 \varepsilon_0}{\partial T^2}. \tag{22}$$

Figure 6(c) presents the results for the specific heat versus temperature given by the transfer-integral calculations. One notes an extremely sharp peak at $T = 278$ K.

It corresponds to the penetration of the lowest eigenvalue ε_0 in the continuum band, which is associated with a sharp knee in the variation versus T of the lowest eigenvalue of the transfer operator, as attested by Fig. 6(a). In fact, the amplitude of this peak seems to be essentially limited by the temperature step used in the calculation. Finally, in Fig. 6(b), we show how the energy per site varies with temperature. The most striking feature conveyed by Fig. 6(b) is the sudden rise in U. The steeply rising coexistence segment of the curve in Fig. 6(c) is not strictly vertical because of the numerical method to compute the lowest eigenvalues (one can note that it is not a finite size effect because the eigenvalues and therefore all thermodynamic functions are obtained in the thermodynamic limit).

In addition, we made some numerical simulation of this system using molecular dynamics simulation at constrained temperature with the Nosé-Hoover method [30–34,13] on a Connection Machine 5 with 16 384 units. It is possible then to study the histogram of the value of the different site y_n for different temperatures. The simulation were first integrated during 20 000 time units in order to reach an equilibrium state and then we continued to integrate the equations, saving the position of all the sites with a regular time interval. On the Fig. 7 we plot the fraction of units that have a value of y exceeding a threshold 1.5 Å. The transition is extremely rapid in comparison with the harmonic case [13]. These values are then used to make the histogram of the different available positions. We plot the results on Fig. 8. One sees that at low temperature the histogram has a sharp peak around the value zero, which means that the chain is in the well of the Morse potential. For higher values of

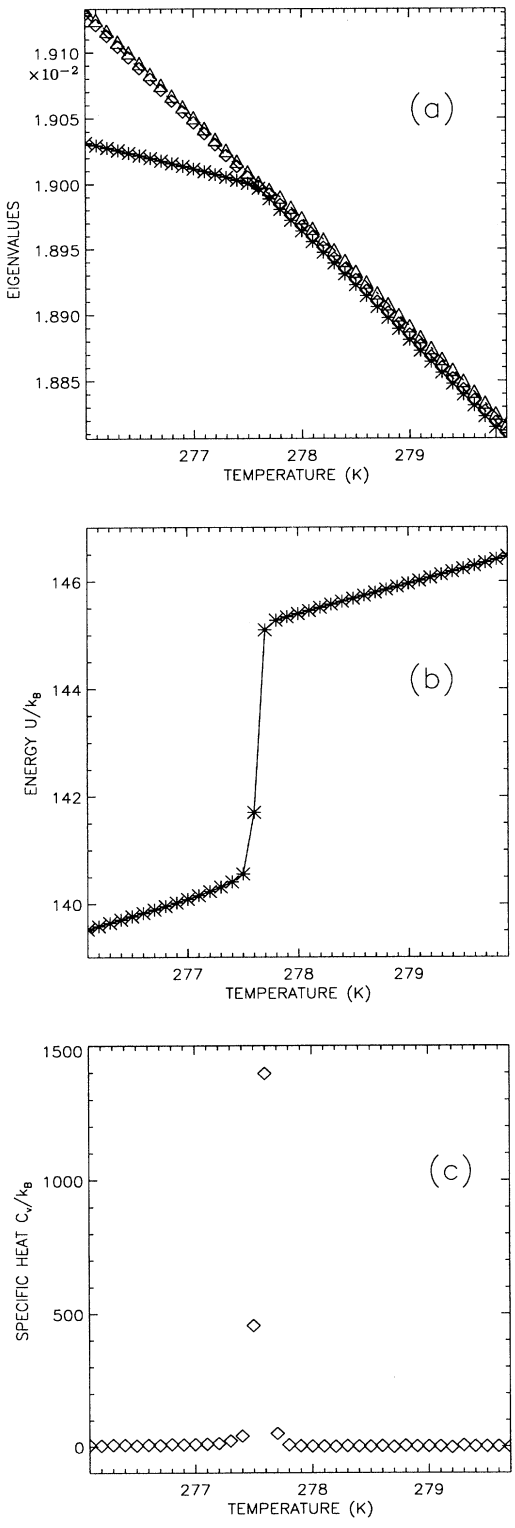

FIG. 6. (a) The three lowest eigenvalues of the transfer integral operator. The asterisk corresponds to ε_0, the diamond to ε_1, and the triangle to ε_2. (b) The evolution of the energy versus T. (c) The evolution of the specific heat on the same interval of temperature. The parameters are $\alpha = 0.35$, $D = 0.03$ eV, $a = 4.5$ Å^{-1}, $K = 0.06$ eV/Å, $\rho = 1.0$, and $m = 300$ amu.

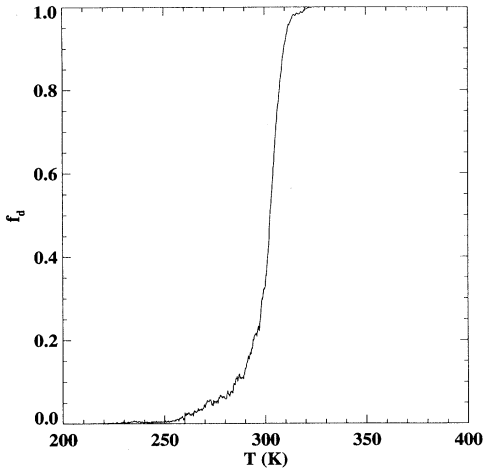

FIG. 7. Variation of the fraction of cells that are denaturated f_d vs temperature. f_d is calculated by counting the number of base pairs that have a mean stretching exceeding a threshold of 1.5 Å. The parameters are $\alpha = 0.35$, $D = 0.03$ eV, $a = 4.5$ Å^{-1}, $K = 0.06$ eV/Å, $\rho = 1$, and $m = 300$ amu.

the temperature, all the particles are on the plateau. For an intermediate range of temperature, parts of the particles are still in the well, as attested by the small peak of the dashed line around zero, although other parts are on the plateau. This is also reminiscent of a phase coexistence phenomenon.

Naturally at this step, because the model remains short ranged, the question arises whether it is a real first-order transition because of the sharpness of the peak in the specific heat. At first sight this seems to contradict the

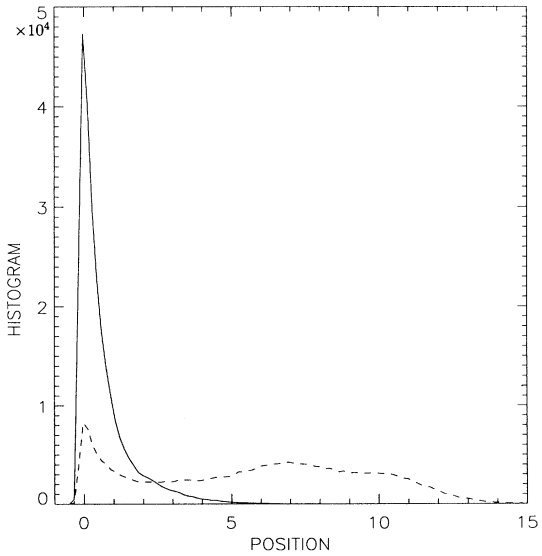

FIG. 8. Histogram of the open sites for two different temperatures. The solid curve corresponds to a temperature of 300 K and the dashed line corresponds to 310 K. The parameters are $\alpha = 0.35$, $D = 0.03$ eV, $a = 4.5$ Å^{-1}, $K = 0.06$ eV/Å, $\rho = 1.0$, and $m = 300$ amu.

well-known result that there are no phase transitions in one-dimensional (1D) systems, with short-range interactions [35]. One can easily illustrate this theorem with the oft-repeated example of the linear chain Ising model (see, for example, Ref. [36]). Let us assume that an ordered state exists below $T_c > 0$ and that there exists a phase transition at temperature T_c. Then for $T < T_c$, let us flip half the chain to assume an opposite polarity, which clearly increases the enthalpy by an amount $2J$, which is the enthalpy required to change the relative polarity of a nearest-neighbor pair of spins. However, since it can be carried out in N ways (according to which of the N bonds is flipped) there will be a resultant increase in entropy of order $(\ln N)$ and the Gibbs potential $G = U - TS$ will decrease rather than increase. Thus the system is unstable against such flips and we conclude that for an infinite system an ordered phase for $T > 0$ cannot exist. Therefore, no spontaneous magnetization can appear in a linear Ising model. The preceding derivation clearly breaks down in the presence of an external field since the two states do not correspond anymore to the same energy level. In that case, the energy increases with N and not with $\ln N$.

Theoretical questions related to the phase-transition problem in a double polymer chain (such as the DNA molecule) have been discussed many times in the literature [37–39]. The process of splitting of a long double molecule into individual filaments is under certain conditions [37] indeed a phase transition. Using a simple model and only nearest-neighbor interaction, one can exhibit examples [38,40] that demonstrate that a phase transition is not forbidden in a 1D system since, to our knowledge, the demonstration of the theorem is only valid for potential using differences of the positions [11].

VI. DISCUSSION AND CONCLUSION

To elucidate the reason of this transition, we can perform the same type of calculations with other similar Hamiltonians. Our results show that the transition requires *simultaneously* two properties of the model. One is a property of the coupling along the chain and the other one is a characteristic of the on-site potential. Let us discuss the coupling first.

As already explained, when $\alpha = 0$ (the coupling interaction is then harmonic) the spectrum of the TI operator shows a smooth evolution of the lowest eigenvalue toward the continuum; simultaneously the eigenfunction ϕ_0 shows a smooth evolution toward delocalization by forming a side maximum that grows. The transition is clearly not a first-order transition [see Figs. 2(a) and 2(c)].

To show that the behavior of the model is sensitive to the type of dependence upon y_n of the effective coupling constant, we studied the model with the following coupling potential:

$$W_1(y_n, y_{n-1}) = \frac{K}{2}\left(1 + \rho e^{-\alpha|y_n - y_{n-1}|}\right)(y_n - y_{n-1})^2. \tag{23}$$

Figure 9(a) shows the specific heat versus the temperature. The curve corresponds to a broad peak, due to a 1D Schottky anomaly. We note then that the plus sign is of importance in the exponential. In a mean field approximation, with a minus sign, the coupling constant is not a function of the mean stretching, contrary to our Hamiltonian.

We studied also the coupling potential

$$W_2(y_n, y_{n-1}) = \frac{K}{2}\left(1 + \rho - \rho e^{-\alpha(y_n + y_{n-1})}\right) \times (y_n - y_{n-1})^2. \tag{24}$$

That case has the plus sign in the exponential, but the prefactor of the quadratic term $(y_n - y_{n-1})^2$ increases from $\frac{1}{2}K$ to $\frac{1}{2}K(1+\rho)$, when either or both base pair are stretched. Therefore, a base pair that is in the vicinity of an open site has greater vibrational frequencies, which increases its contribution to the free energy since the free energy of a single classical harmonic oscillator is $\mathcal{F} = -k_B T \ln[2\pi k_B T/\omega]$. Figure 9(b) shows that with the W_2 coupling there is only an extremely smooth maximum of specific heat. On the other hand, the coupling potential (2) allows a lower coupling along the strands when the base pair are stretched and so gives the bases more freedom to move independently from each other, causing an entropy increase, which drives the transition.

The second essential point is the coexistence of a plateau in the Morse potential. One could think of a model where the two possible states are both confined states. This would be the case, for instance, for a double well on-site potential such as the well-known ϕ^4 potential

$$V_1(y) = D(y^2 - 1)^2 \tag{25}$$

instead of the Morse potential. This model has no transition and this appears again on the specific heat, which has simply a small peak [Fig. 9(c)]. One could think of coming closer to the case of the Morse potential by using a potential that has two equilibrium positions with different energies such that the asymmetric ϕ^4 potential

$$V_2(y) = \frac{D}{2}[3(y^2 - 1)^2 + y]. \tag{26}$$

Again there is no sharp transition as shown in Fig. 9(d) [41]. These two cases suggest that the plateau of the Morse potential is really required and this is supported by two arguments.

(i) In a previous study of an entropy-driven transition with an on-site potential having a ϕ^6 shape (with only minima confined by a potential energy increasing to infinity for $y \to \pm\infty$), Morris and Gooding did *not* find a transition in the limit of a one-dimensional model [5]. They analyzed their results by showing that instead of a crossing of two eigenvalues of the transfer integral operator leading to degeneracy they had only an avoided crossing as shown in Fig. 10(a). With a potential unbounded for $y \to \pm\infty$, the transfer integral operator has only a set of *discrete* eigenvalues that depend on T and the avoided crossing can be repeated to avoid any degeneracy of eigenvalues as shown in Fig. 10(b). But with a

potential having a *plateau*, there is a *qualitative* change because the transfer operator has a *continuum* part in its spectrum. As shown in Fig. 10(c), if a discrete eigenvalue tends to penetrate into the continuum, the crossing cannot be avoided unless one digs a "channel" in the continuum to allow the curve $\varepsilon_0(T)$ to pass through without intersecting with the continuum. This is of course not a mathematical proof of the existence of the transition because we cannot, from such a topological argument, definitely exclude a sharp bend of $\varepsilon_0(T)$ before it reaches the continuum as shown in Fig. 10(d). But, if it were the case it would be difficult to explain the anomaly in the density of states that appears in the continuum in our Fig. 4 along the continuation of the $\varepsilon_0(T)$ curve.

(ii) The transition is only possible if an entropy increase can balance the energy increase shown in Fig. 6(b) in order to reduce sufficiently the free energy of the denaturated phase for $T > T_c$. As discussed above, the special nonlinear coupling, which gives the particle more freedom to move in the denaturated state, tends to favor an entropy increase. But the plateau of the Morse potential is also crucial because when the whole atomic chain is on the plateau, the absence of confining potential (contrary to the ϕ^4 or the ϕ^6 potential) allows them to explore almost freely a very large domain in the phase space. In fact, although we are working with a one-dimensional model because the on-site variable can be labeled by only one index (along the particle chain), in the denaturated state, the chain of particles evolves actually in a two-dimensional space as illustrated in Fig. 11. This fact was recognized earlier by Kosevich *et al.* [38] when they studied a one-dimensional DNA model made of segments having a finite number of possible orientations. The calculation of the number of configurations

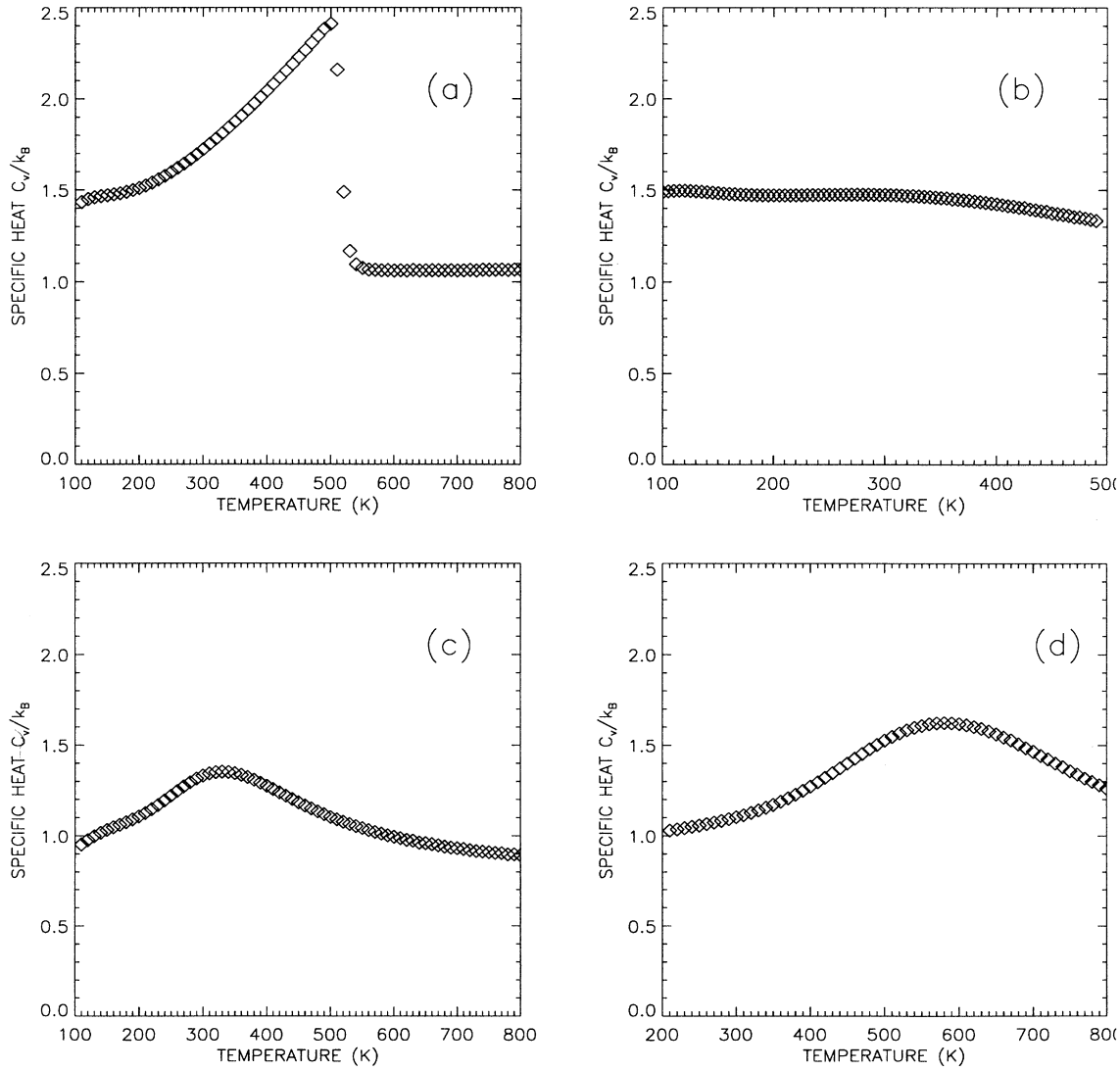

FIG. 9. Specific heat in k_B unit versus the temperature. (a) and (b) present the cases with the coupling potentials (24) and (23), respectively, (c) presents the case with the ϕ^4 potential and the anharmonic potential (2), and (d) presents the case with the asymmetric ϕ^4 potential and the anharmonic potential (2).

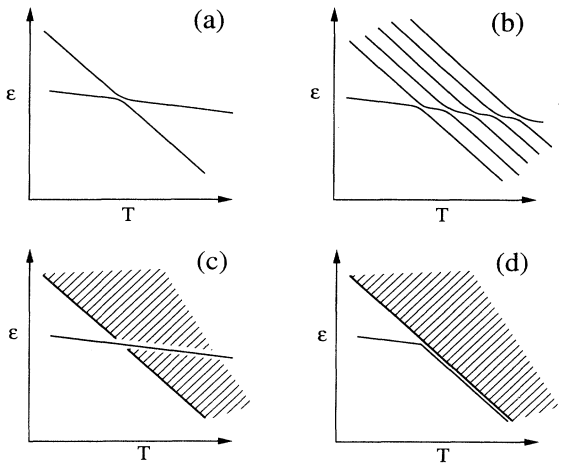

FIG. 10. Qualitative pictures showing how a degeneracy could be avoided in the eigenvalues of the transfer operator when they vary versus T: (a) avoided crossing of two discrete states, (b) sequence of avoided crossing when an isolated eigenvalue penetrates into a domain that contains many discrete eigenvalues, (c) penetration of an isolated eigenvalue in a continuum, and (d) avoided crossing by abrupt bending of the variation of an isolated eigenvalue approaching a continuum.

of the model to get the partition function lead them to consider random walks in two or three dimensions.

In summary, we showed that the cooperativity effects that we introduced previously [14] in the model of DNA denaturation through purely nearest-neighbor coupling terms can change dramatically the transition. With this interaction, the system presents an extremely sharp entropy-driven transition. The self-consistent phonons calculations can be performed analytically up to second order. The fact that even at this order the SCP calculation cannot describe correctly the transition shows the essential role of the nonlinear effects in the vicinity of the transition. With the use of two different methods, we are able to obtain exact numerical values of the thermodynamical functions. The transition is related to two main features of the Hamiltonian: on the one hand, it is necessary to introduce a nonlinear coupling constant that decreases in the denaturated phase to provide a large entropy; on the other hand, the on-site potential must be bounded with a plateau. The approach that we presented here agrees with recent views on structural phase transition in elastic media that stress that intrinsic nonlinear features characterize the physics of these transformations and extend the standard soft mode picture [1,7].

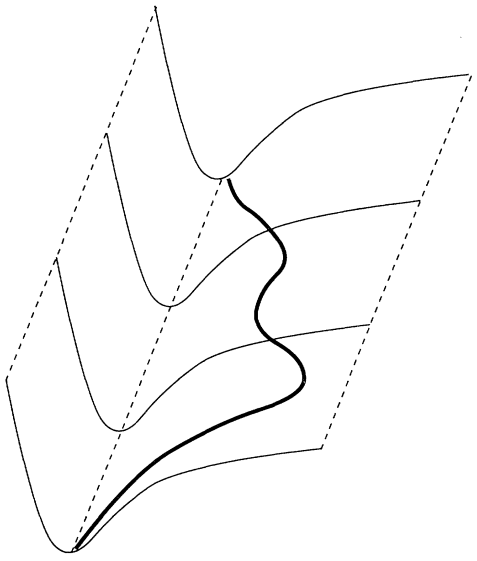

FIG. 11. Schematic view showing how the chain of particles (represented here by the heavy line) can explore a two-dimensional space in the denaturated state when the on-site potential has a plateau.

The statistical mechanics results show that it is possible to design a simple one-dimensional model that provides a good description of the DNA denaturation transition as it is observed experimentally on short chains. From the point of view of the physical motivations of this work, the next part is to study the effects of the disorder (the sequence for the DNA model) on the denaturation. Indeed, to investigate the activation mechanism it is crucial to take into account the nonuniformity because the transcription is induced by promoter regions. This is a very sensitive test of the model because it is well documented experimentally and the cooperativity of the transition has been shown experimentally to depend drastically on the sequence and the ionic content of the solution. At this point numerical simulation is absolutely crucial since very little is known on disordered nonlinear systems. Experimentally the thin details of the denaturation curves result from statistics on the millions of molecules present in the vessel. We can only test our model against these results if we can generate numerically very accurate denaturation curves, i.e., if we can obtain extremely good statistics in the thermalized numerical simulations. Only studies of many, sufficiently large, independent samples over a long time can provide significant results. Preliminary studies show that the model can exhibit a fine structure in the denaturation curve that is similar to the structure observed experimentally.

This study should give us the elements to define the role of the base sequence (i.e., the genetic code) in the localization phenomenon. Our guess is that the combination of the nonlinearity and the disorder will give us the opportunity to understand the main features of the denaturation process. We expect this connection to play an important role in the mechanism of genetic activation, where the specificity is crucial for both the binding of specific proteins to DNA and the transport of such proteins from the promoter to the fragments corresponding to the genes. Work in this direction is currently in progress.

ACKNOWLEDGMENTS

The authors wish to acknowledge helpful and instructive discussions with A. R. Bishop. They are also grateful

to J.-L. Barrat, P. C. W. Holdworth, A. M. Kosevich, J. Piasecki, and C. R. Willis. The authors thank CEC for financial support through Contract No. SC1-CT91-0705, the Advanced Computing Laboratory at Los Alamos, and the CNCPST at Jussieu in Paris. This work was partially performed on computing resources located at these facilities.

APPENDIX: CALCULATION OF THE MEAN VALUES FOR THE SCP METHOD

In this appendix we present only the main results, useful to obtain the expression of the mean value of the perturbative potential $\langle V_{\rm pert}\rangle$. The calculations are particularly tedious. We introduce the matrix $\mathbf{M}$, with $M_{i,j} = (\frac{\Omega^2}{2} + \phi)\delta_{i,j} - \frac{\phi}{2}(\delta_{i,j+1} + \delta_{i,j-1})$ as we did in the harmonic case [13].

Let us define the quadratic form

$$Q = \sum_{i,j} \mathbf{M}_{i,j} u_i u_j - \sum_i h_i(u_i - u_{i+1}) + \sum_i c_i u_i \tag{A1}$$

with $c_i = 0$, except $c_i = \alpha/\beta$ if $i = k, k+1, \ell, \ell+1$. We have then

$$\Delta = \langle (u_l - u_{l+1})^2 (u_k - u_{k+1})^2 e^{-\alpha(u_k + u_{k+1} + u_l + u_{l+1})} \rangle \tag{A2}$$

$$= \frac{\int \prod_i du_i (u_l - u_{l+1})^2 (u_k - u_{k+1})^2 \exp\left(-\beta \sum_{i,j} \mathbf{M}_{i,j} u_i u_j - \alpha(u_k + u_{k+1} + u_l + u_{l+1})\right)}{\int \prod_i du_i \exp\left(-\beta \sum_i \mathbf{M}_{i,j} u_i u_j\right)} \tag{A3}$$

$$= \frac{1}{\beta^2 \mathcal{Z}(\mathbf{0},\mathbf{0})} \left[\frac{\partial^4}{\partial h_k^2 \partial h_l^2} \int \prod_i du_i e^{-\beta Q}\right]\Bigg|_{\mathbf{h}=\mathbf{0}}. \tag{A4}$$

We introduce then the variable $v_i = u_i - a_i$, where $\mathbf{a}$ is chosen so that the linear term of the quadratic form vanishes. It gives

$$\Delta = \frac{1}{\beta^2} * \frac{\partial^4 e^{\beta\, {}^t\mathbf{a}\mathbf{M}\mathbf{a}}}{\partial h_k^2 \partial h_l^2}\Bigg|_{\mathbf{h}=\mathbf{0}} \tag{A5}$$

$$= \Big\{ 2(2\langle u_k u_\ell\rangle - \langle u_k u_{\ell+1}\rangle - \langle u_\ell u_{k+1}\rangle)^2 \Big[1 - 2\alpha^2(\langle u_{k+1} u_\ell\rangle - \langle u_k u_{\ell+1}\rangle)^2\Big] + \Big[2(\langle u^2\rangle - \langle v^2\rangle) + \alpha^2(\langle u_{k+1} u_\ell\rangle - \langle u_k u_{\ell+1}\rangle)^2\Big]^2 \Big\} e^{\alpha^2(2\langle u^2\rangle + 2\langle v^2\rangle + 2\langle u_k u_\ell\rangle + \langle u_{k+1} u_\ell\rangle + \langle u_{\ell+1} u_k\rangle)}. \tag{A6}$$

If $\alpha = 0$, it reads

$$\langle (u_k - u_{k+1})^2 (u_\ell - u_{\ell+1})^2 \rangle = 2\Big[2(\langle u^2\rangle - \langle v^2\rangle)^2 + (2\langle u_k u_\ell\rangle - \langle u_k u_{\ell+1}\rangle - \langle u_\ell u_{k+1}\rangle)^2\Big]. \tag{A7}$$

Using the same quadratic form, but $c_i = 0$, except where $c_k = c_{k+1} = \frac{\alpha}{\beta}$, we obtain

$$\Gamma = \langle (u_k - u_{k+1})^2 (u_\ell - u_{\ell+1})^2 e^{-\alpha(u_k + u_{k+1})} \rangle \tag{A8}$$

$$= \frac{1}{\beta^4} \frac{\partial^4 e^{\beta\, {}^t\mathbf{a}\mathbf{M}\mathbf{a}}}{\partial h_k^2 h_\ell^2} \tag{A9}$$

$$= 2[(2\langle u_k u_\ell\rangle - \langle u_k u_{\ell+1}\rangle - \langle u_\ell u_{k+1}\rangle)^2 + 2(\langle u^2\rangle - \langle v^2\rangle)^2] e^{\alpha^2(\langle u^2\rangle + \langle v^2\rangle)}. \tag{A10}$$

Using the same quadratic form, but $c_i = 0$, except where $c_k = c_{k+1} = \frac{\alpha}{\beta}$, $c_\ell = \frac{a}{\beta}$, it reads

$$\Theta = \langle (u_k - u_{k+1})^2 e^{-a u_\ell} e^{-\alpha(u_k + u_{k+1})} \rangle \tag{A11}$$

$$= \frac{1}{\beta^2} \frac{\partial^2 e^{\beta\, {}^t\mathbf{a}\mathbf{M}\mathbf{a}}}{\partial h_k^2} \tag{A12}$$

$$= [2(\langle u^2\rangle - \langle v^2\rangle) + a^2(\langle u_{k+1} u_\ell\rangle - \langle u_k u_\ell\rangle)^2] \times e^{\alpha^2(\langle u^2\rangle + \langle v^2\rangle) + \frac{a^2}{2}\langle u^2\rangle + 2a\alpha(\langle u_k u_\ell\rangle + \langle u_{k+1} u_\ell\rangle)}. \tag{A13}$$

The two particular cases $\alpha = 0$ and $a = 0$ are useful for the calculation. Using the same quadratic form, but $c_i = 0$, except where $c_k = c_{k+1} = \frac{\alpha}{\beta}$, $c_\ell = \frac{a}{\beta}$, it reads

$$\Xi = \langle (u_k - u_{k+1})^2 u_\ell^2 e^{-\alpha(u_k+u_{k+1})} \rangle \tag{A14}$$

$$= \frac{1}{\beta^4} \frac{\partial^4 e^{\beta\, {}^t\mathbf{aMa}}}{\partial h_k^2 c_\ell^2} \tag{A15}$$

$$= 2\Big\{ (\langle u_{k+1}u_\ell \rangle - \langle u_k u_\ell \rangle)^2 + (\langle u^2 \rangle - \langle v^2 \rangle) \times \Big[\langle u^2 \rangle + \alpha^2 (\langle u_\ell u_k \rangle + \langle u_\ell u_{k+1} \rangle)^2 \Big] \Big\} e^{\alpha^2(\langle u^2 \rangle + \langle v^2 \rangle)}. \tag{A16}$$

When $\alpha = 0$, it reads

$$\langle (u_k - u_{k+1})^2 u_\ell^2 \rangle = 2\Big[(\langle u_k u_\ell \rangle - \langle u_{k+1} u_\ell \rangle)^2 + \langle u^2 \rangle (\langle u^2 \rangle - \langle v^2 \rangle) \Big]. \tag{A17}$$

Finally, introducing the expressions

$$\mu = \frac{K - \phi}{2}, \quad \gamma = \frac{K\rho}{2} e^{-2\alpha\eta},$$

$$\lambda = De^{-2a\eta}, \quad \delta = 2De^{-a\eta},$$

$$\sigma = aD\Big[2(a - \alpha) e^{-2a\eta + 2a^2\langle u^2 \rangle} + (2\alpha - a) e^{-a\eta + \frac{a^2}{2}\langle u^2 \rangle} \Big]$$

to simplify the calculation, we can then obtain the mean value of the square of the perturbative potential

$$\begin{aligned}
\frac{\langle V_{\text{pert}} \rangle}{N} &= \frac{\langle (H - H_0)^2 \rangle}{N} \\
&= N\Big[\sigma^2 \langle u^2 \rangle^2 - 2\lambda\sigma \langle u^2 \rangle e^{2a^2\langle u^2 \rangle} + 2\delta\sigma \langle u^2 \rangle e^{\frac{a^2}{2}\langle u^2 \rangle} \Big] \\
&\quad + \sum_k \Big(2\mu^2 \Big[2(\langle u^2 \rangle - \langle v^2 \rangle)^2 + (2\langle u_k u_\ell \rangle - \langle u_k u_{\ell+1} \rangle - \langle u_\ell u_{k+1} \rangle)^2 \Big] \\
&\quad + \gamma^2 \Big\{ 2(2\langle u_k u_\ell \rangle - \langle u_k u_{\ell+1} \rangle - \langle u_\ell u_{k+1} \rangle)^2 - 4\alpha^2 (2\langle u_k u_\ell \rangle - \langle u_k u_{\ell+1} \rangle - \langle u_\ell u_{k+1} \rangle)(\langle u_{k+1} u_\ell \rangle - \langle u_k u_{\ell+1} \rangle)^2 \\
&\quad + \Big[2(\langle u^2 \rangle - \langle v^2 \rangle) + \alpha^2 (\langle u_{k+1} u_\ell \rangle - \langle u_k u_{\ell+1} \rangle)^2 \Big]^2 \Big\} e^{\alpha^2(2\langle u^2 \rangle + 2\langle v^2 \rangle + 2\langle u_k u_\ell \rangle + \langle u_{k+1} u_\ell \rangle + \langle u_{\ell+1} u_k \rangle)} \\
&\quad + \lambda^2 e^{4a^2\langle u^2 \rangle} e^{4a^2 \langle u_k u_\ell \rangle} + \delta^2 e^{a^2\langle u^2 \rangle} e^{a^2 \langle u_k u_\ell \rangle} + 2\sigma^2 \langle u_k u_\ell \rangle^2 - 2\lambda\delta e^{\frac{5a^2}{2}\langle u^2 \rangle} e^{2a^2 \langle u_k u_\ell \rangle} - 8\lambda\sigma a^2 e^{2a^2\langle u^2 \rangle} \langle u_k u_\ell \rangle^2 \\
&\quad + 2\delta\sigma a^2 e^{\frac{a^2}{2}\langle u^2 \rangle} \langle u_k u_\ell \rangle^2 + 4\mu\gamma \Big[(2\langle u_k u_\ell \rangle - \langle u_k u_{\ell+1} \rangle - \langle u_\ell u_{k+1} \rangle)^2 + 2(\langle u^2 \rangle - \langle v^2 \rangle)^2 \Big] e^{\alpha^2(\langle u^2 \rangle + \langle v^2 \rangle)} \\
&\quad + 4\mu\lambda \Big[\langle u^2 \rangle - \langle v^2 \rangle + a^2 (\langle u_{k+1} u_\ell \rangle - \langle u_k u_\ell \rangle)^2 + a^2 (\langle u_{\ell+1} u_k \rangle - \langle u_k u_\ell \rangle)^2 \Big] e^{2a^2\langle u^2 \rangle} \\
&\quad - \mu\delta \Big[4(\langle u^2 \rangle - \langle v^2 \rangle) + a^2 (\langle u_{k+1} u_\ell \rangle - \langle u_k u_\ell \rangle)^2 + a^2 (\langle u_{\ell+1} u_k \rangle - \langle u_k u_\ell \rangle)^2 \Big] e^{\frac{a^2}{2}\langle u^2 \rangle} \\
&\quad - 2\mu\sigma \Big[(\langle u_k u_\ell \rangle - \langle u_{k+1} u_\ell \rangle)^2 + (\langle u_k u_\ell \rangle - \langle u_{\ell+1} u_k \rangle)^2 + 2\langle u^2 \rangle (\langle u^2 \rangle - \langle v^2 \rangle) \Big] \\
&\quad + 2\gamma\lambda \Big[\langle u^2 \rangle - \langle v^2 \rangle + 2a^2 (\langle u_{k+1} u_\ell \rangle - \langle u_k u_\ell \rangle)^2 \Big] e^{\alpha^2(\langle u^2 \rangle + \langle v^2 \rangle) + 2a^2\langle u^2 \rangle + 4a\alpha(\langle u_k u_\ell \rangle + \langle u_{k+1} u_\ell \rangle)} \\
&\quad + 2\gamma\lambda \Big[\langle u^2 \rangle - \langle v^2 \rangle + 2a^2 (\langle u_{\ell+1} u_k \rangle - \langle u_k u_\ell \rangle)^2 \Big] e^{\alpha^2(\langle u^2 \rangle + \langle v^2 \rangle) + 2a^2\langle u^2 \rangle + 4a\alpha(\langle u_k u_\ell \rangle + \langle u_{\ell+1} u_k \rangle)} \\
&\quad - \gamma\delta \Big[2(\langle u^2 \rangle - \langle v^2 \rangle) + a^2 (\langle u_{k+1} u_\ell \rangle - \langle u_k u_\ell \rangle)^2 \Big] e^{\alpha^2(\langle u^2 \rangle + \langle v^2 \rangle) + \frac{a^2}{2}\langle u^2 \rangle + 2a\alpha(\langle u_k u_\ell \rangle + \langle u_{k+1} u_\ell \rangle)} \\
&\quad - \gamma\delta \Big[2(\langle u^2 \rangle - \langle v^2 \rangle) + a^2 (\langle u_{\ell+1} u_k \rangle - \langle u_k u_\ell \rangle)^2 \Big] e^{\alpha^2(\langle u^2 \rangle + \langle v^2 \rangle) + \frac{a^2}{2}\langle u^2 \rangle + 2a\alpha(\langle u_k u_\ell \rangle + \langle u_{\ell+1} u_k \rangle)} \\
&\quad - 2\gamma\sigma \Big\{ (\langle u_{k+1} u_\ell \rangle - \langle u_k u_\ell \rangle)^2 + (\langle u_{\ell+1} u_k \rangle - \langle u_k u_\ell \rangle)^2 \\
&\quad + (\langle u^2 \rangle - \langle v^2 \rangle) \Big[2\langle u^2 \rangle + \alpha^2 (\langle u_\ell u_k \rangle + \langle u_\ell u_{k+1} \rangle)^2 + \alpha^2 (\langle u_\ell u_k \rangle + \langle u_k u_{\ell+1} \rangle)^2 \Big] \Big\} e^{\alpha^2(\langle u^2 \rangle + \langle v^2 \rangle)} \Big).
\end{aligned}$$

This expression allows us to compute the value of the second-order correction to the free energy (14).

[1] J. A. Krumhansl and R. J. Gooding, Phys. Rev. B **39**, 3047 (1989).

[2] J. R. Morris and R. J. Gooding, Phys. Rev. Lett. **65**, 1769 (1990).

[3] J. R. Morris and R. J. Gooding, Phys. Rev. B **43**, 6057 (1991).

[4] J. R. Morris and R. J. Gooding, J. Stat. Phys. **67**, 471 (1992).

[5] J. R. Morris and R. J. Gooding, Phys. Rev. B **46**, 8733 (1992).

[6] W. C. Kerr and M. J. Rave, Phys. Rev. B **48**, 16 234 (1993).

[7] W. Kerr *et al.*, Phys. Rev. B **45**, 7036 (1992).
[8] R. J. Gooding and J. R. Morris, Phys. Rev. E **47**, 2934 (1993).
[9] J. F. Nagle, Am. J. Phys. **36**, 1114 (1968).
[10] C. Kittel, Am. J. Phys. **37**, 917 (1969).
[11] L. Van Hove, Physica **16**, 137 (1950).
[12] W. Saenger, *Principles of Nucleic Acid Structure* (Springer-Verlag, Berlin, 1984).
[13] T. Dauxois, M. Peyrard, and A. R. Bishop, Phys. Rev. E **47**, 684 (1993).
[14] T. Dauxois, M. Peyrard, and A. R. Bishop, Phys. Rev. E **47**, R44 (1993).
[15] M. Peyrard and A. R. Bishop, Phys. Rev. Lett. **62**, 2755 (1989).
[16] C. Reiss (private communication).
[17] T. Dauxois and M. Peyrard, Phys. Rev. Lett. **70**, 3935 (1993).
[18] M. Techera, L. L. Daemen, and E. W. Prohofsky (unpublished).
[19] M. Techera, L. L. Daemen, and E. W. Prohofsky, in *Nonlinear Coherent Structures in Physics and Biology*, edited by M. Remoissenet and M. Peyrard (Springer, New York, 1991), p. 87.
[20] S. Ma, *Statistical Mechanics* (World Scientific, Singapore, 1991).
[21] R. P. Feynman, *Statistical Mechanics* (Benjamin, New York, 1972).
[22] C. Grojean, Ecole Normale Supérieure de Lyon Rapport de Magistère, 1994 (unpublished).
[23] D. J. Scalapino, M. Sears, and R. A. Ferrel, Phys. Rev. B **6**, 3409 (1972).
[24] J. A. Krumhansl and J. R. Schrieffer, Phys. Rev. B **11**, 3535 (1975).
[25] J. F. Currie *et al.*, Phys. Rev. B **22**, 47 (1980).
[26] S. E. Trullinger and K. Sasaki, Physica D **28**, 181 (1988).
[27] T. Schneider and E. Stoll, Phys. Rev. B **22**, 5317 (1980).
[28] R. Courant and D. Hilbert, *Methods of Mathematical Physics* (Wiley, New York, 1989).
[29] Practically, the transition is between a mean stretching close to zero and a value related to the half-size of the finite spatial resolution domain.
[30] S. Nosé, Mol. Phys. **52**, 255 (1984).
[31] S. Nosé, J. Chem. Phys. **81**, 511 (1984).
[32] W. G. Hoover, Phys. Rev. A **31**, 1695 (1985).
[33] S. Nosé, Phys. Rev. E **47**, 164 (1993).
[34] N. Theodorakopulos and M. Peyrard (unpublished).
[35] E. Lieb and D. C. Mattis, *Mathematical Physics in One Dimension* (Academic, New York, 1966).
[36] H. E. Stanley, *Phase Transitions and Critical Phenomena* (Oxford University Press, New York, 1987).
[37] B. Zimm, J. Chem. Phys. **33**, 1349 (1960).
[38] A. M. Kosevich, V. L. Galkin, and I. N. Nechiporenko, Zh. Eksp. Teor. Fiz. **66**, 261 (1974) [Sov. Phys. JETP **39**, 124 (1975)].
[39] Y. Z. Chen and E. W. Prohofsky, Biopolymers **66**, 202 (1994).
[40] A. M. Kosevich (private communication).
[41] There is a small peak in the specific heat at very low temperature not related to the same transition and not represented in order to avoid confusion.